

Numerical Modelling of Disordered Magnetic Systems: $\text{La}_{2-x}\text{Sr}_x\text{CoO}_4$

M. Rotter¹

¹*martin_rotter@mcphase.de, Neutron Science Laboratory,
Institute for Solid State Physics, University of Tokyo, Tokai 319-1106,
Japan / McPhase Project www.mcphase.de, Dresden, Germany*

(Dated: September 17, 2018)

Magnetic properties of $\text{La}_{2-x}\text{Sr}_x\text{CoO}_4$ have been modelled using McPhase for different doping levels x . Footprints of different interactions, such as local single ion anisotropy and variations in the exchange interactions have been identified in the profile of the diffuse elastic neutron scattering cross section. The role of quantum fluctuations in the formation of the hourglass spectrum is discussed.

PACS numbers: 71.70.Ch, 74.70.Dd, 75.10.Dg, 78.70.Nx

I. INTRODUCTION

Charge, spin and orbital order in layered transition metal oxides may be influenced considerably by electron doping resulting in exotic and complex physical properties, which have high potential for technological application.

This study focuses on $\text{La}_{2-x}\text{Sr}_x\text{CoO}_4$, which has been studied experimentally recently. There is large consensus, that in this system the charge order is static and stable up to at least room temperature^{1,2}. However, it is matter of ongoing debate, if charge stripes are present in this system or not. For example, the famous hourglass spectrum for $x \sim 0.4$ can be interpreted based on a (i) frustrated charge stripe³⁻⁵ and a (ii) frustrated checkerboard charge order⁶⁻⁸. Indeed, no clear experimental evidence for the existence of charge stripes in $\text{La}_{2-x}\text{Sr}_x\text{CoO}_4$ has been found and thus it is interesting to investigate by model calculations, if the existence of charge stripes is indeed needed in order to interpret all available experimental data. In an attempt to answer this question, extensive simulations using the McPhase 5.2 software suite⁹ (www.mcphase.de) have been performed. In the next section the basic model will be described, followed by a presentation of selected calculation results. The last section is devoted to the modelling of quantum fluctuations using a magnetic cluster approach. The input files for McPhase and summary logbooks of the calculations are available as a supplementary material to this article under www.mcphase.de/lSCO.zip

II. DESCRIPTION OF THE MODEL

A. Generation of Frustrated Checkerboard Charge Order Pattern

Statistical/random disordered checkerboard charge order pattern of size 30x30 were generated from Monte-Carlo simulations similar to^{5,7} (Drees et al. and Andrade et al.) using the Metropolis algorithm for the two dimensional Ising model. Only one potential for Coulomb repulsion of two adjacent Co^{3+} and another for steric re-

pulsion of Co^{2+} ions with large ionic radii has been considered. A longitudinal external field was used to tune the number of Co^{3+} ions according to the desired doping level x . For the simulation of diffuse scattering an average of 64 configurations was performed.

B. Modelling the Magnetic Properties

Magnetism was modeled by introducing antiferromagnetic exchange interactions between the Co^{2+} ions i, j with spin operators $\hat{\mathbf{S}}^i$ and $\hat{\mathbf{S}}^j$, respectively (the Co^{3+} ions were assumed to be in the low spin state and treated as nonmagnetic):

$$H_{ex} = -\frac{1}{2} \sum_{i,j} J(ij) \hat{\mathbf{S}}^i \cdot \hat{\mathbf{S}}^j \quad (1)$$

The simplest model is obtained by introducing two exchange constants. We set $J(100) = -9.5$ meV as observed in the parent phase¹⁰ with $x = 0$. Note, the "100" in $J(100)$ refers to the pseudotetragonal unit cell of the high temperature tetragonal phase. In addition, $J(200) = -1.4$ meV is considered, if the interstitial (100) neighbour ion is Co^{3+} , this value is taken from the pure checkerboard charge ordered phase² with $x = 0.5$.

An effort was made to extend previous work on the dilute systems, where the Co^{2+} spin had been modelled using an effective $S=1/2$. Here, the properties of the Co^{2+} ion were calculated based on the same coupling scheme as used in^{2,10} including crystal field and spin orbit interaction parameters $B_2^0 = 14.6$ meV, $B_4^0 = -1.35$ meV, $B_4^4 = -8.0$ meV, $\lambda = -22.1$ meV, for notation see¹¹.

$$H_{Co}^i = \sum_{lm} B_l^m O_l^m(\hat{\mathbf{L}}^i) + \lambda \hat{\mathbf{L}}^i \cdot \hat{\mathbf{S}}^i \quad (2)$$

Note that the crystal field anisotropy will tend to align the magnetic moments perpendicular to c . In order to enable calculations involving many ions, the spin matrices of the exchange Hamiltonian (1) were projected to the 4

lowest lying eigenstates $|\alpha\rangle$ ($\alpha = 1, \dots, 4$ with energies E_α) of the single ion Hamiltonian (2) of the Co ions:

$$\hat{\mathbf{S}}^i \sim \sum_{\alpha, \beta} |\alpha\rangle \langle \alpha | \hat{\mathbf{S}}^i | \beta \rangle \langle \beta| \quad (3)$$

With this substitution (3) inserted in the exchange interaction (1) the total Hamiltonian becomes:

$$H = H_{ex} + \sum_{i, \alpha} |\alpha\rangle E_\alpha \langle \alpha| \quad (4)$$

In several figures of this article calculated neutron scattering cross sections are shown in dipole approximation. Energies and Intensities of the modes were evaluated by dynamical matrix diagonalisation (for details see Rotter et al.⁹). The general expression for the double differential magnetic scattering cross section for unpolarised neutrons has been given frequently in literature (see e.g.¹²):

$$\frac{d^2\sigma_{\text{mag}}}{d\Omega dE'} = \frac{k'}{k} \left(\frac{\gamma r_0}{2\mu_B} \right)^2 \sum_{\alpha, \beta=1,2,3} (\delta_{\alpha\beta} - \frac{Q_\alpha Q_\beta}{|\mathbf{Q}|^2}) \times \frac{1}{2\pi\hbar} \int_{-\infty}^{+\infty} dt e^{i\omega t} \sum_{nn'} e^{-W_n(Q) - W_{n'}(Q)} e^{-i\mathbf{Q} \cdot (\mathbf{R}_n - \mathbf{R}_{n'})} \times \langle \hat{M}_\alpha^{n\dagger}(t, \mathbf{Q}) \hat{M}_\beta^{n'}(0, \mathbf{Q}) \rangle_{T,H} \quad (5)$$

In (5) \mathbf{k} and \mathbf{k}' denote the wave vector of the incoming and scattered neutron, respectively. The total magnetic cross section is $4\pi(\gamma r_0)^2 = 4\pi \left(\frac{\hbar\gamma e^2}{mc^2} \right)^2 = 3.65$ barn. $\hbar\omega = E - E'$ and $\mathbf{Q} = \mathbf{k} - \mathbf{k}'$ denote the energy and momentum transfer. $\exp(-W_n(Q))$ is the Debye-Waller factor of the atom number n .

The magnetic scattering operator $\hat{\mathbf{M}}(\mathbf{Q})$ was obtained from the spin $\hat{\mathbf{S}}$ by applying an anisotropic Landé factor $g_x = g_y = 2.79$, $g_z = 2$. In the calculation of the cross section the form factor and the Debye Waller factors were not considered (set to 1), i.e.

$$\hat{M}_\alpha(\mathbf{Q}) \sim g_\alpha \hat{S}_\alpha \quad (6)$$

The resolution function for elastic scattering was assumed to be Gaussian with a width of $\Delta h = \Delta k = 0.03$ in both h and k direction, for inelastic scattering a Q -resolution of $\Delta h = 0.05$ and an energy resolution $\Delta E = 4$ meV was used.

In this way it is not only possible to model the hour-glass spectrum for $x = 0.4$, but also to investigate it's evolvment for different x quantitatively. For example, the optical modes observed for $x = 0.5$ may be modeled (not possible within an effective $S=1/2$ approach). Figs. 1 to 6 show the results of such calculations.

Still, there are major drawbacks of this model:

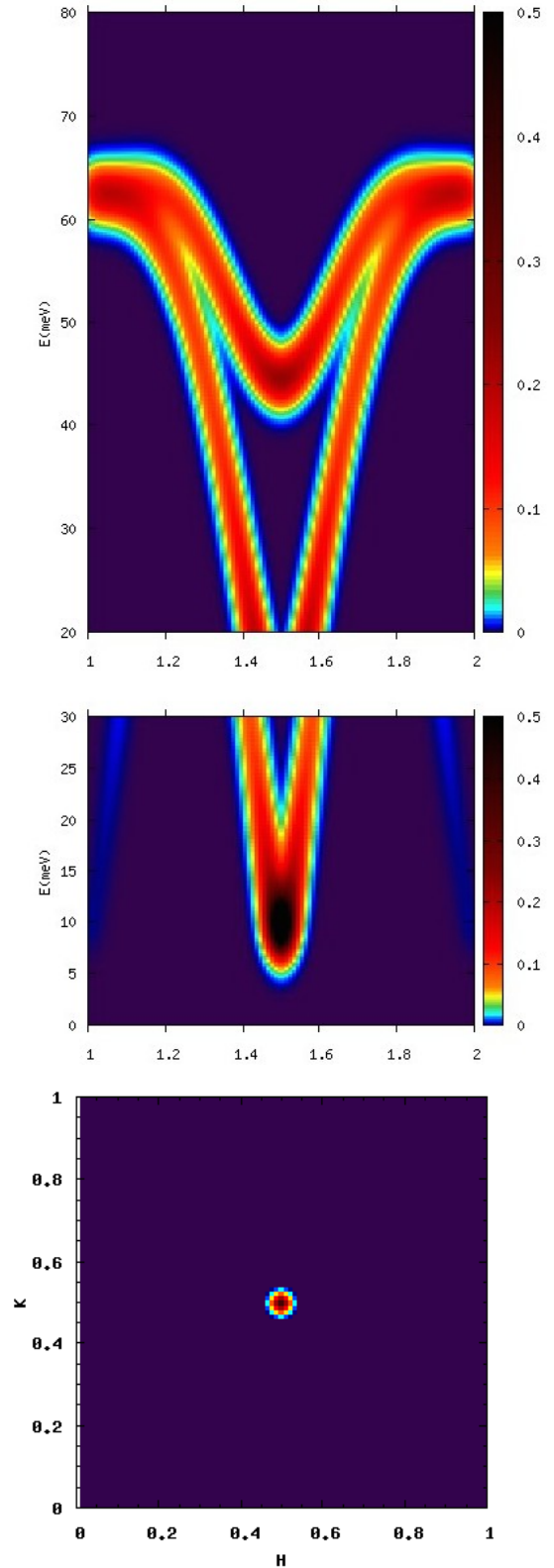


FIG. 1: Simulated inelastic (top: along (h 0.5 0), middle: along (hh0) and elastic (bottom: (hk0) plane) magnetic neutron pattern for $x=0$.

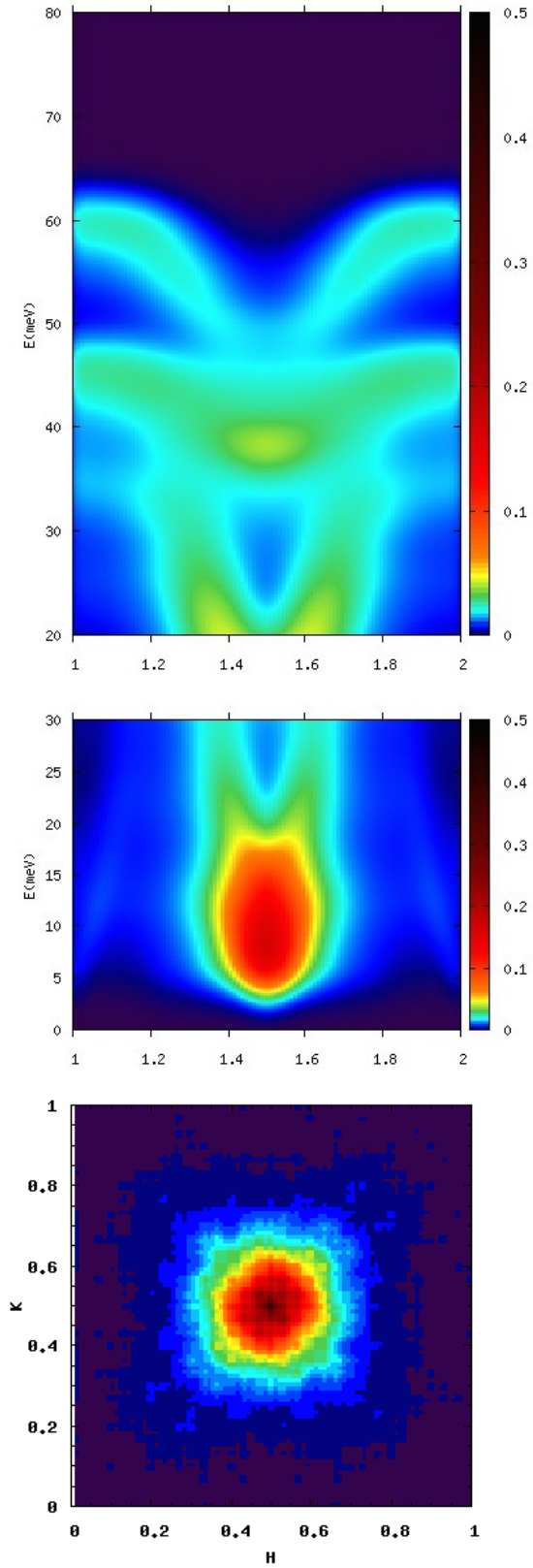


FIG. 2: Simulated inelastic (top: along $(h\ 0.5\ 0)$, middle: along $(hh0)$ and elastic (bottom: $(hk0)$ plane) magnetic neutron pattern for $x=0.25$

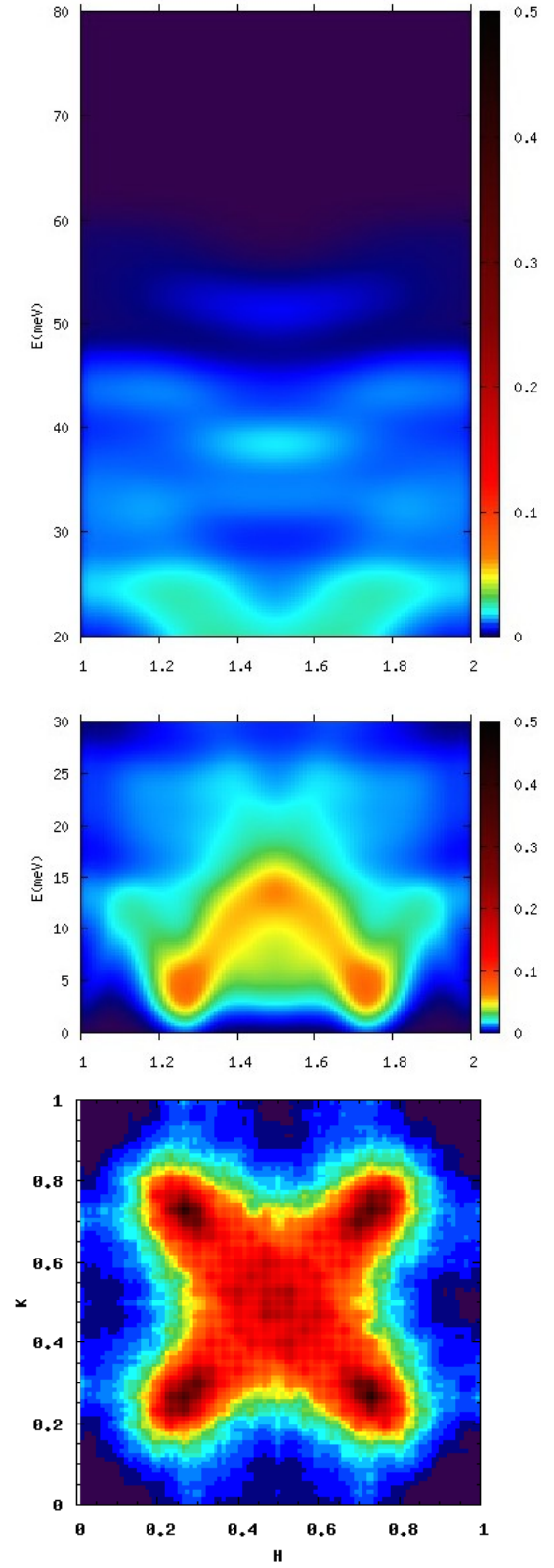


FIG. 3: Simulated inelastic (top: along $(h\ 0.5\ 0)$, middle: along $(hh0)$ and elastic (bottom: $(hk0)$ plane) magnetic neutron pattern for $x=0.4$

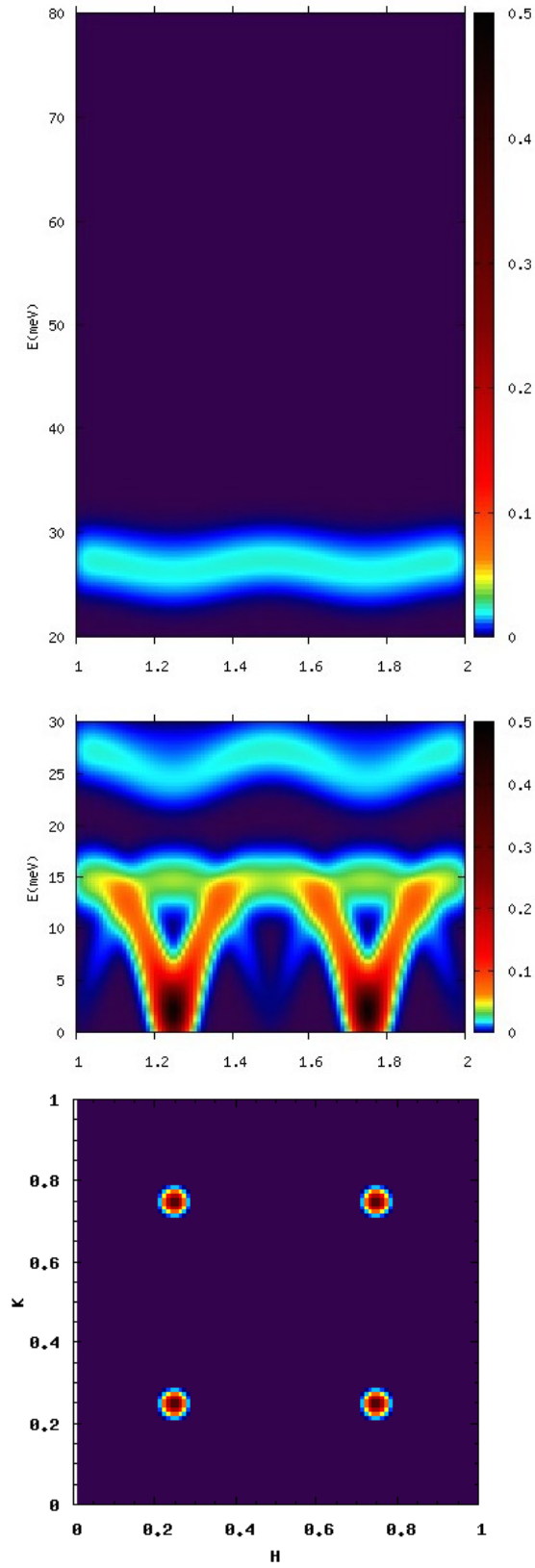


FIG. 4: Simulated inelastic (top: along $(h\ 0.5\ 0)$, middle: along $(hh0)$ and elastic (bottom: $(hk0)$ plane) magnetic neutron pattern for $x=0.5$

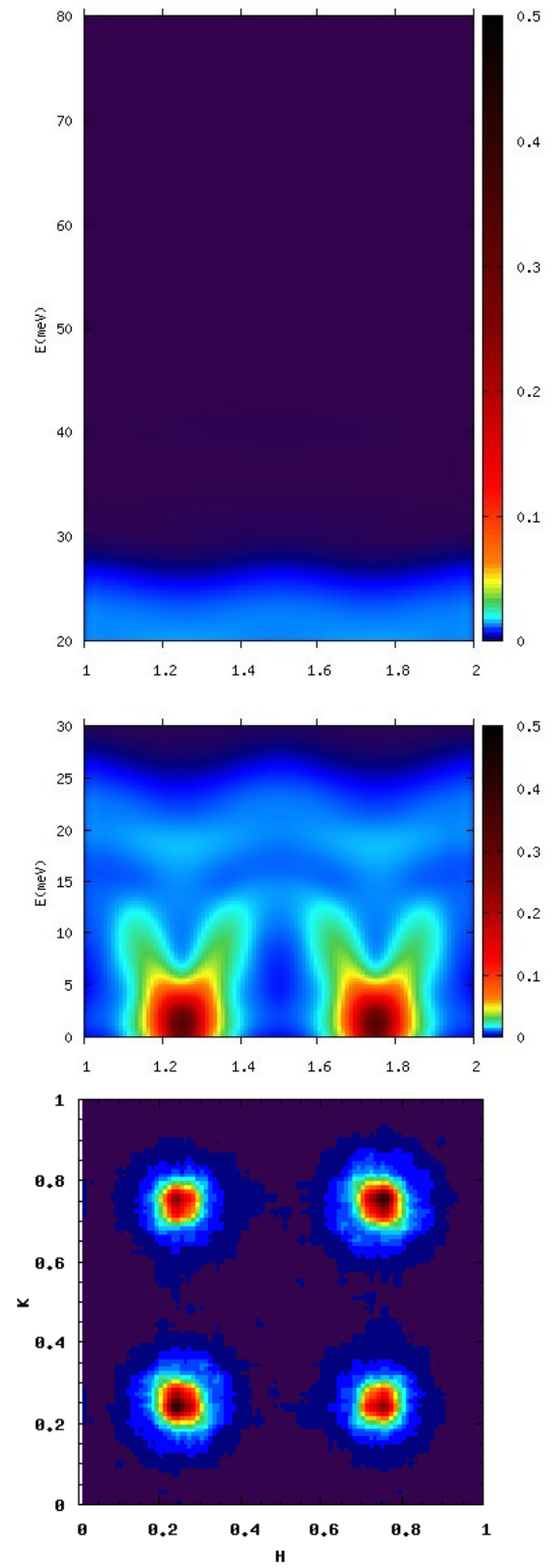


FIG. 5: Simulated inelastic (top: along $(h\ 0.5\ 0)$, middle: along $(hh0)$ and elastic (bottom: $(hk0)$ plane) magnetic neutron pattern for $x=0.6$

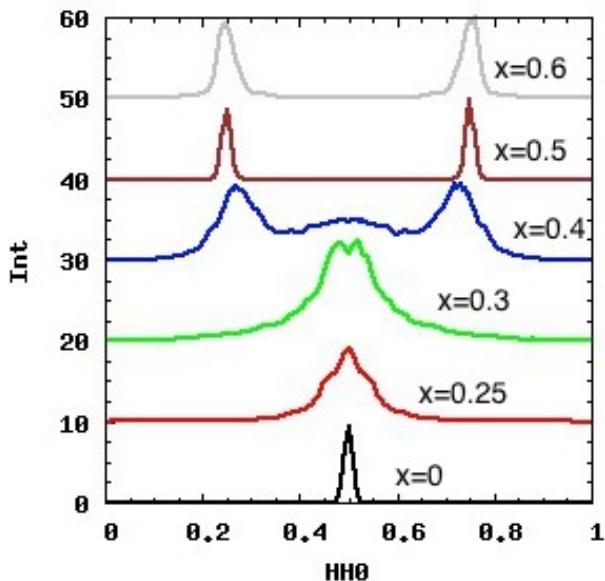


FIG. 6: Simulated elastic magnetic neutron pattern along $hh0$ for different x .

- Note that the gap in the excitation spectra was produced by introducing an anisotropy field on each Co^{2+} site similar to^{2,10}: the calculated mean fields were simply increased by 1%. However, the source of this anisotropy field remains unclear.
- In comparison to experimental data for $x = 0.25$ it is evident, that the width of the diffuse scattering is too small and the fourfold star like structure is missing³. However, more recent experimental data are in better agreement¹⁸.
- For $x = 0.4$ there is too strong magnetic diffuse scattering around $(0.5, 0.5, 0)$ in comparison to the experiment^{6,13}.

In the following sections we report an attempt to improve the understanding of anisotropy and of the diffuse scattering within the framework of a frustrated checkerboard charge order model.

III. INVESTIGATION OF THE ROLE OF SINGLE ION ANISOTROPY IN THE FORMATION OF THE EXCITATION GAP

The role of single ion anisotropy in $\text{La}_{2-x}\text{Sr}_x\text{CoO}_4$ was investigated. In $\text{La}_{2-x}\text{Sr}_x\text{CoO}_4$ it is known that the magnetic moments order perpendicular to the c -axis. This anisotropy can be produced by a crystal field B_2^0 parameter as described in section II B. Yet, such anisotropy will not lead to a gap in the excitation spectra (13 meV for $x = 0$, 3 meV for $x = 0.5$), because the moment direction within the ab plane is not fixed leading to a Goldstone mode.

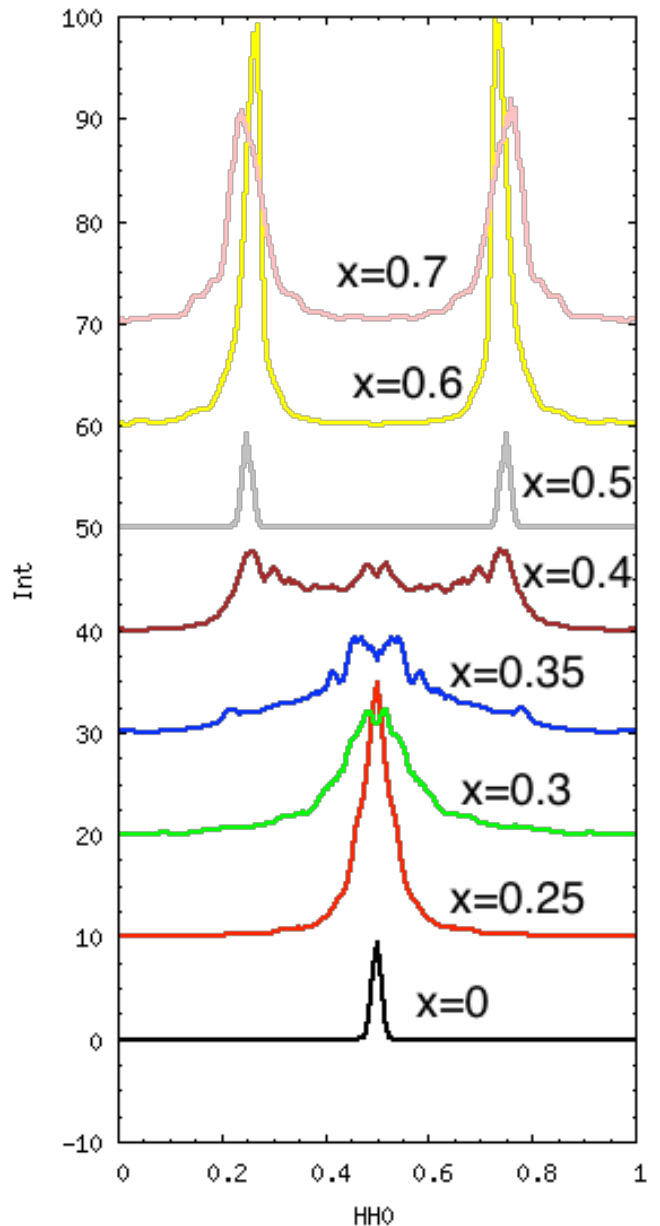


FIG. 7: Simulated elastic magnetic neutron pattern along $hh0$ for different x .

One possible cause of additional single ion anisotropy is the low temperature orthorhombic (LTO) distortion of $\text{La}_{2-x}\text{Sr}_x\text{CoO}_4$ ¹³ with a unit cell approximately $\sqrt{2} \times \sqrt{2}$ the tetragonal unit cell. This orthorhombic symmetry may lead (among others) to an additional crystal field parameter $B_2^2(s)$. In order to reproduce the experimental gaps, we set this parameter $B_2^2(s) = -3.97$ meV for $x = 0$ and $B_2^2(s) = -1.63$ meV for $x = 0.5$. The calculated spectra for $x=0$ and $x=0.5$ are nearly identical with those shown in figs. 1 and 4.

Fig. 7 shows the results of magnetic elastic scattering using an average of 4 charge order grids, demonstrating

that there is no improvement in the description of the experimental data with respect to the previous model.

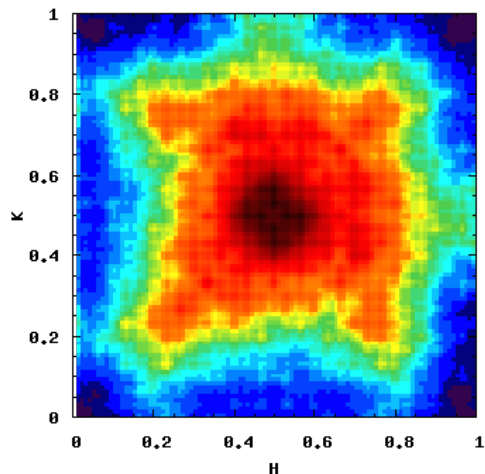


FIG. 8: Simulated elastic magnetic neutron pattern in the $(hk0)$ plane for $x=0.3$ including local variations in Co-O distance.

Moreover, despite its success in describing the gap the real cause of anisotropy has to be more complex than a simple introduction of an orthorhombic $B_2^2(s)$ parameter: (i) for $x = 0.5$ no orthorhombic distortion has been observed at any temperature (ii) also the parent phase $x = 0$ is not orthorhombic at low temperature, it exhibits a low temperature tetragonal phase (LTT). Characteristic is the tilt of the octahedron in the low temperature tetragonal (LTT) and low temperature orthorhombic (LTO) phases. The tilts about the $[1, -1, 0]$ direction form an antiferrodistortive structural arrangement¹⁴. These tilts produce more complex single ion anisotropy than just a nonzero $B_2^2(s)$ parameter. Therefore, in the next step single ion anisotropy is described by a tilt of the octahedron. The additional nonzero crystal field parameters were estimated from the point charge model and doubled to effectively account for bonding effects. The tilt was assumed to vary depending on the local concentration of Co^{3+} ions. For $x = 0$ a tilt of 12 deg and for $x = 0.5$ a tilt of 10 deg is found to yield the experimental anisotropy gaps.

IV. INVESTIGATION OF THE ROLE OF LOCAL VARIATIONS IN OXYGEN POSITIONS

It is a widely accepted assumption that for Co^{3+} based oxides with octahedral coordination the cobalt-oxygen (Co-O) distance will determine the spin state of Co^{3+} . The prototype system LaCoO_3 with a temperature induced low spin (LS) to high spin (HS) transition exhibits a Co-O distance of 1.925 \AA ¹⁵. The Co-O distances in La_2CoO_4 are above this critical value and thus doping with Sr should induce a HS state of Co^{3+} in

contrast to the widely used assumption, that Co^{3+} in $\text{La}_{2-x}\text{Sr}_x\text{CoO}_4$ is in its LS nonmagnetic state. Another peculiarity of $\text{La}_{2-x}\text{Sr}_x\text{CoO}_4$ is that fact, that on doping with Sr the lattice shrinks, although Sr^{2+} has a larger ionic radius than La^{3+} .

From these observations it seems possible, that there are local variations in Co-O distances depending on the ionic radius of the Co ion. Actually such variations are needed in order to justify the steric repulsion of adjacent Co^{2+} used in the model for the checkerboard charge order (see section II A). According to crystal field theory a local variation in Co-O distance should also induce a corresponding crystal field anisotropy. Moreover, local variations of oxygen positions might also affect the hopping and thus influence the exchange interactions between the magnetic ions. In a series of model calculations these effects were investigated and the footprints in the diffuse magnetic scattering were identified. An example of such a simulation is shown in fig. 8.

A. Local variations in Crystal Field Anisotropy

The local additional crystal field anisotropy of Co^{2+} ions induced by an asymmetric Co^{3+} neighbourhood is described by a local variation in the crystal field parameter B_2^2 , which was estimated from the point charge model assuming a shift of oxygen positions of 0.13 \AA according to the difference in ionic radii of Co^{2+} (0.88 \AA) and Co^{3+} (0.75 \AA for the HS state, 0.69 \AA for LS). If there is only one Co^{3+} neighbour this anisotropy will tend to align moments perpendicular to the direction of the Co^{3+} neighbour. In this way the nano clusters of the parent ($x = 0$) compound will tend to have their moments aligned parallel to their major axis. For example if such a cluster is elongated along (100), moments will also tend to point along (100) and the $J(100)$ interactions will induce a propagation of $(0.5 \text{ k } 0)$, k depending on the actual shape of the cluster. Due to the polarisation factor the intensity will be larger at $(0.5 \text{ 1 } 0)$ than at $(0.5 \text{ 0 } 0)$ leading to an asymmetry in the diffuse scattering shown in fig. 8 - the "star" is not symmetric, but there is more intensity around $(0.5 \text{ 0.8 } 0)$ and $(0.8 \text{ 0.5 } 0)$ than around $(0.5 \text{ 0.2 } 0)$ and $(0.2 \text{ 0.5 } 0)$, respectively. However, such an asymmetry in the diffuse scattering has not been found in the experiment^{3,6}. Thus local variations of oxygen positions of the order of 0.1 \AA are unlikely in $\text{La}_{2-x}\text{Sr}_x\text{CoO}_4$.

B. Local variations in Exchange Interactions

Moreover, some effect of different Co ion size on exchange interactions between a nearest neighbour pair of Co^{2+} ions was taken into account in the simulation shown in fig. 8: if on one side of the pair there is a Co^{3+} nearest neighbour, the interaction was reduced from -9.5 to -2.5 meV, if on both sides there are Co^{3+} nearest neighbours

it is taken to be +0.5 meV. Thus bonds perpendicular to the major axis of a parent phase nano cluster are weaker and the cluster can be viewed approximately as a series of one dimensional chains with nearest neighbour interaction $J(100) = -9.5$ meV along the major axis. This will lead to diffuse intensity stripes along $(0.5 \ k \ 0)$ and $(h \ 0.5 \ 0)$, which are also not observed in the experiment. Note that in the simulation shown in fig. 8 these intensity stripes are visible only at $(0.5 \ 1 \ 0)$ and $(1 \ 0.5 \ 0)$ and not at $(0.5 \ 0 \ 0)$ and $(0 \ 0.5 \ 0)$ because of the local variations of single ion anisotropy described above. Thus also the absence of local variations in exchange interactions contradict the assumption of local variations of oxygen positions in $\text{La}_{2-x}\text{Sr}_x\text{CoO}_4$.

V. SPIN NEMATIC INTERACTIONS

Up to now we have assumed a nonzero crystal field anisotropy in the ab plane for all x in $\text{La}_{2-x}\text{Sr}_x\text{CoO}_4$. However, because of the absence of a tilt of the octahedron this assumption is not justified for $x = 0.5$. Thus it is necessary to look out for other possible sources of anisotropy, which could lead to the observed anisotropy gap. Recently, Soda et al.¹⁶ pointed out that spin nematic interactions of the form $-1/2 \sum_{ij} K(ij) O_2^2(s)(\hat{\mathbf{L}}_i) \cdot O_2^2(s)(\hat{\mathbf{L}}_j)$ may induce an anisotropy gap. In the following we used such interactions with $K(200) = 0.05$ meV and found that in this way the anisotropy gap for $x = 0.5$ can be successfully described. Thus in our final approach to anisotropy investigation spin nematic interactions are used. $K(200)$ is put nonzero only, if a Co^{3+} ion is at the intermediate (100) position mediating the interaction.

In addition, depending on the number of adjacent Co^{3+} ions the tilt angle induced anisotropy is linearly scaled from 12 deg (zero adjacent Co^{3+}) to 0 deg (4 adjacent Co^{3+} ions).

VI. INCREASING FRUSTRATION BY VARIATIONS IN (110) AND (200) INTERACTIONS

The discrepancy in diffuse scattering between experimental data and results of the model calculation are (i) the width and anisotropy of the diffuse scattering for $x = 0.25$ and (ii) the intensity around $(1/2 \ 1/2 \ 0)$ for $x = 0.4$. The description of these two features of the experimental data may be significantly improved by an increase in frustration via introducing variations in the exchange couplings $J(110)$ and $J(200)$.

In the studies of Babkevich¹⁰ and Helme² it was found that $J(110)$ is zero for $x = 0$ and $x = 0.5$ - yet it is unclear, why the simple estimate based on exchange paths involving a single Co^{3+} bonding orbital $J(110) = 2 \cdot J(200)$ does not apply. Here we introduce nonzero $J(110) = -2$ meV only, if exactly one of the two (100) and (010) adjacent neighbours is Co^{3+} and the other is

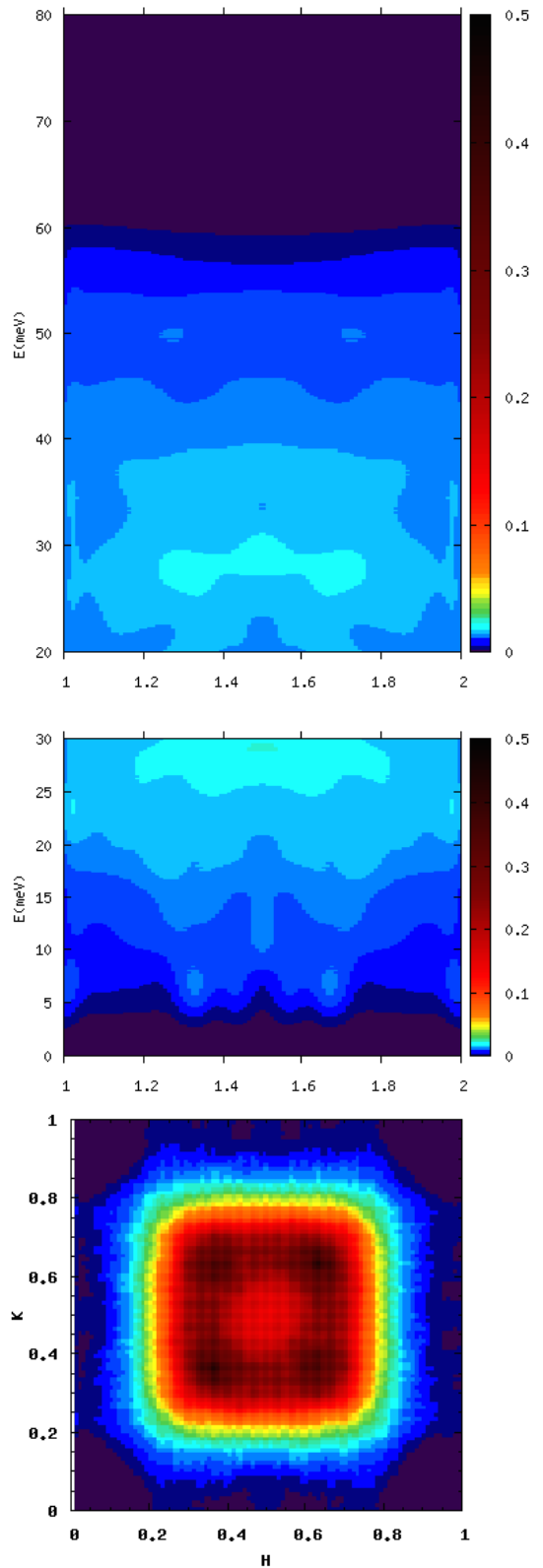


FIG. 9: Simulated inelastic (top: along $(h \ 0.5 \ 0)$, middle: along $(hh0)$ and elastic (bottom: $(hk0)$ plane) magnetic neutron pattern for $x=0.25$

Co^{2+} . This rule will yield zero $J(110)$ for the parent compound $x = 0$ and also for the checkerboard charge order $x = 0.5$. The size of $J(200)$ is assumed to vary proportional to the amount of Co^{2+} ions in the neighbourhood, i.e. we choose $J(200) = -1.4$ meV if 0,1 or 2 out of 6 NN are Co^{2+} , $J(200) = -3.5$ meV if 3 or 4 out of 6 NN are Co^{2+} and $J(200) = -7.0$ meV if 5 or 6 out of 6 NN are Co^{2+} .

Fig. 9 shows the result of such a simulation. The elastic diffuse magnetic scattering shows a fourfold pattern, which does not resemble the perfect "star" observed in the experiment³. The inelastic pattern for $x = 0.25$ has no similarity to the hourglass, because the huge magnetic frustration leads to a lot of broad diffuse scattering and prevents a resonance like peak.

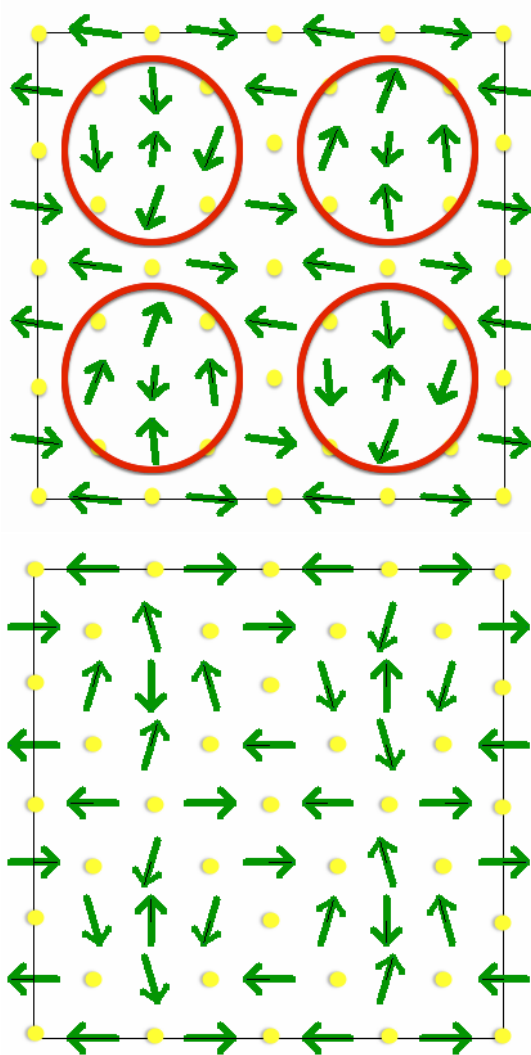


FIG. 10: Regular doped checkerboard charge order pattern corresponding to $x=0.4375$. Red circles indicate the magnetic clusters which consist of 5 strongly interacting Co^{2+} ions. The calculated spin structure using a cluster approach (top) is compared to that obtained with a standard single ion calculation (bottom).

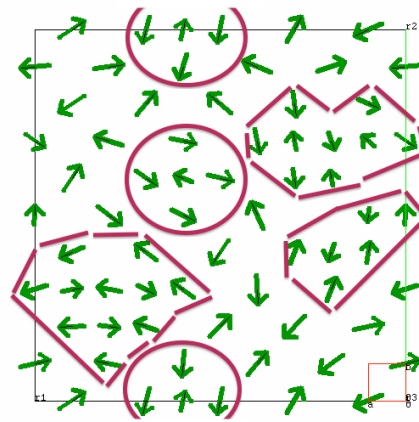


FIG. 11: Magnetic order on a 10x10 frustrated checkerboard charge order pattern corresponding to $x=0.42$. Red circles indicate the magnetic nano clusters. The calculated spin structure using a cluster approach is shown.

VII. BEYOND SINGLE ION THEORY - SOME CLUSTER CALCULATIONS

In order to investigate the role of quantum fluctuations it is possible to make a first step by forming out of strongly interacting adjacent Co^{2+} ions a magnetic cluster. For computational reasons we revert to the simplest model described by⁷ (Drees et al.), which has been shown to predict an hourglass spectrum (anisotropic effective $S=1/2$ without in plane anisotropy $\langle S_x \rangle = \langle S_y \rangle = 1.5$, $\langle S_z \rangle = 1.3$, $J(100) = -5.8$ meV, $J(200) = -0.85$ meV). If checkerboard charge order would not freeze out some stochastic charge configuration it might be possible to observe regular charge order pattern, for example in a 8×8 superstructure as shown in fig. 10 and corresponding to $x = 7/16 = 0.4375$. For this pattern the magnetic properties were calculated (i) using exact diagonalisation of the five-ion clusters indicated by the red circles in fig. 10(top) and doing a mean field random phase approximation (MF-RPA) for the weak interactions between the clusters and the remaining Co^{2+} ions¹⁷, the calculated magnetic moments are indicated by the arrows in fig. 10(top). For comparison, (ii) all Co^{2+} ions were treated separately, see fig. 10 (bottom). The cluster-approach (i) yields a smaller magnetic moment on the central Co^{2+} ion of the cluster.

Therefore it is likely, that quantum fluctuations will tend to suppress $(1/2 \ 1/2 \ 0)$ correlations for $x \sim 0.4$ and that the high intensity, which has been calculated around $(1/2 \ 1/2 \ 0)$ is an artefact of the single ion spin wave or MF-RPA approach. In order to see this effect more quantitatively the model was extended to a grid size of 10×10 and clusters consisting of up to 11 ions. An example of such a grid with clusters is shown in fig. 11. Also here the tendency of smaller moments within the nanocluster can be seen. Fig. 12 compares a diffraction pattern

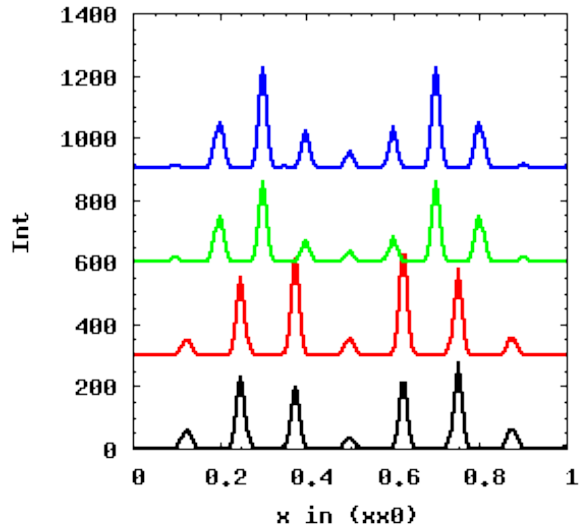


FIG. 12: Diffraction pattern along $(xx0)$ obtained by averaging 8 grids. A calculation with magnetic nano clusters consisting of up to 11 ions is compared to a calculation using single Co^{2+} ions on the same frustrated checkerboard charge order grids corresponding to $x \sim 0.42$. From top to bottom: (i) grid dimension 10×10 , no nano clusters; (ii) same grids as (i) but with nano clusters; (iii) grid dimension 8×8 , no nano clusters; (iv) same grids as (iii) but with nanoclusters.

along $(xx0)$ obtained by averaging 8 grids with magnetic nano clusters (up to 11 ions) to a calculation using single Co^{2+} ions on the same frustrated checkerboard charge order grids corresponding to $x \sim 0.42$. The reduction of the intensity around the center of the plot is clearly visible and stems from nano cluster quantum effects, which are not accounted for in the mean field approach using single Co^{2+} ions.

It has still to be investigated, if also the formation of the resonance like peak is suppressed by such quantum fluctuations and thus the explanation of the hourglass spectrum given in⁷ has to be revised. Therefore the spectral response was calculated for the same grids, which were used to generate fig. 12 and is shown in fig. 13 and fig. 14. The tendency to form a resonance and an hourglass spectrum can clearly be seen in the calculation using nano clusters.

Unfortunately extending this type of calculation to lower concentrations $x < 0.4$ soon runs into the limits of available computational power, because the nano cluster size gets too large. Nevertheless we expect, that

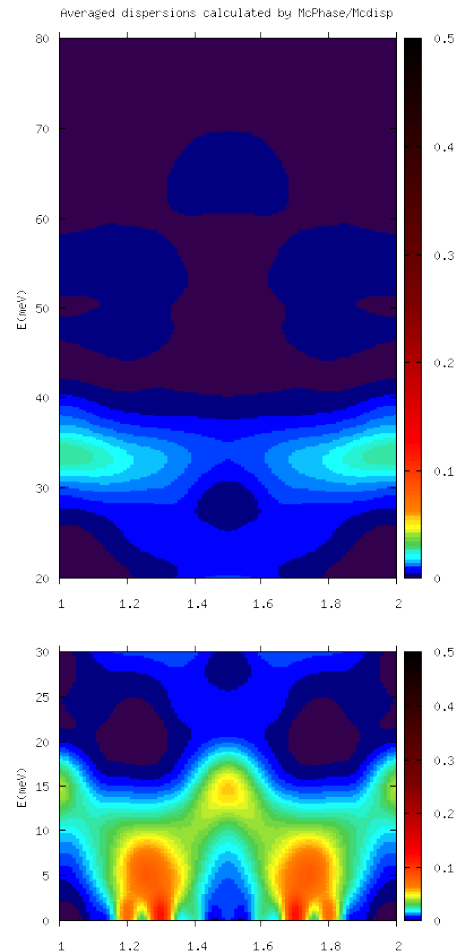


FIG. 13: Averaged spectrum (top) of 8 frustrated checkerboard charge order grids (dimension 10×10) with nano clusters as used in fig. 12 (top). top: along $(h \ 0.5 \ 0)$, bottom: along $(hh0)$

the tendency to reduce the central moments of the nano clusters will persist and will lead to a broadening of the magnetic response down to possibly $x = 0.25$. This might explain, why at such small x a hourglass spectrum has been observed in the experiment, however, without any clear footprint of stripe charge order.

VIII. CONCLUSION

Numerical calculations of the diffuse and inelastic neutron scattering in comparison with experimental data on $\text{La}_{2-x}\text{Sr}_x\text{CoO}_4$ identify spin nematic interactions as a source of anisotropy for $x = 0.5$. Magnetic quantum

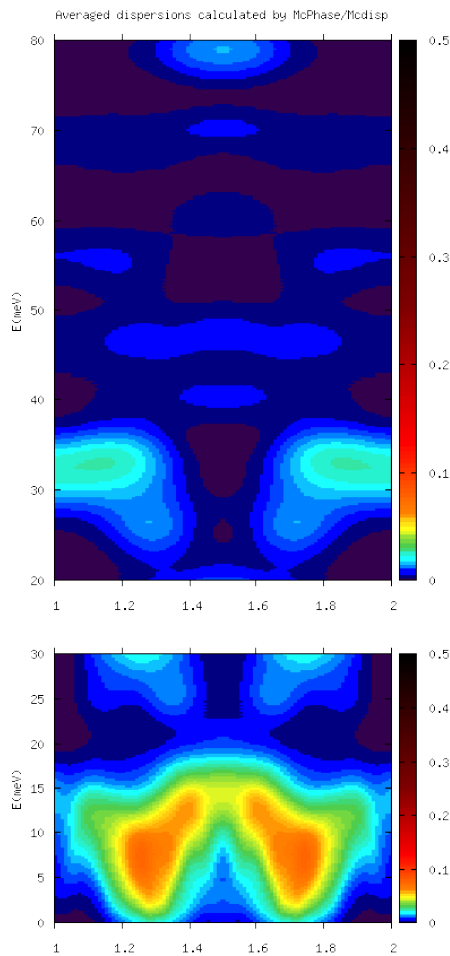


FIG. 14: Averaged spectrum of 8 frustrated checkerboard charge order grids (dimension 10x10, as used in fig. 12 top), however calculated using the standard MF-RPA approach without formation of magnetic nano clusters . top: along $(h\ 0.5\ 0)$, bottom: along $(hh0)$

nano cluster based calculations of spectra on a series of frustrated checkerboard charge order grids for $x \sim 0.42$ show, that quantum fluctuations will destroy short range magnetic order of Co^{2+} rich clusters thus reducing neutron intensity around $(1/2\ 1/2\ 0)$ and possibly leading to an hourglass type of response without charge order stripes for x down to 0.25.

Summa summarum there remain two puzzles in $\text{La}_{2-x}\text{Sr}_x\text{CoO}_4$: (i) the Co^{3+} ions seems to be in a LS state, although the Co-O distance is above the threshold for a HS-LS transition. (ii) Looking at experimental diffuse magnetic scattering data no features for local variations of the in plane oxygen positions of the order of 0.1 Å due to doping can be identified. Therefore the suitability of a nearest neighbour steric repulsion of adjacent Co^{2+} ions in the charge order model may be questioned.

Acknowledgments

The fruitful scientific discussions with Hideki Yoshizawa during my stay at ISSP are highly appreciated. The help of Naoki Kawashima in bringing McPhase to the supercomputer is greatly acknowledged. I wish to thank Jens Jensen for his help in testing the cluster module of McPhase and Alexander C. Komarek for sharing his recent experimental data on a sample with $x = 0.25$. The computation in this work has been done using the facilities of the Supercomputer Center, the Institute for Solid State Physics, the University of Tokyo.

¹ I. A. Zaliznyak, J. P. Hill, J. M. Tranquada, R. Erwin and Y. Moritomo, *Phys. Rev. Lett.* **85**, 4353 (2000)
² L. M. Helme, A. T. Boothroyd, R. Coldea, D. Prabhakaran, C. D. Frost, D. A. Keen, L. P. Regnault, P. G. Freeman, M. Enderle and J. Kulda, *Phys. Rev. B* **80**, 134414 (2009)
³ S. M. Gaw, E. C. Andrade, M. Vojta, C. D. Frost, D. T. Adroja, D. Prabhakaran and A. T. Boothroyd, *Phys. Rev. B* **88**, 165121 (2013)
⁴ A. T. Boothroyd, P. Babkevich, D. Prabhakaran and P. G. Freeman, *Nature* **471**, 341 (2011)
⁵ Eric C. Andrade and Matthias Vojta, *Phys. Rev. Lett.* **109**, 147201 (2012)

⁶ Y. Drees, D. Lamago, A. Piovano and A. C. Komarek, *Nat Commun* **4** (2013)
⁷ Y. Drees, Z. W. Li, A. Ricci, M. Rotter, W. Schmidt, D. Lamago, O. Sobolev, U. Rütt, O. Gutowski, M. Sprung, A. Piovano, J. P. Castellan and A. C. Komarek, *Nat Commun* **5** (2014)
⁸ H. Guo, W. Schmidt, L. H. Tjeng and A. C. Komarek, *physica status solidi (RRL) Rapid Research Letters* **9**, 580 (2015)
⁹ Martin Rotter, Manh Duc Le, Andrew T Boothroyd and Jesus Angel Blanco, *Journal of Physics: Condensed Matter* **24**, 213201 (2012)
¹⁰ P. Babkevich, D. Prabhakaran, C. D. Frost and A. T.

- Boothroyd, *Phys. Rev. B* **82**, 184425 (2010)
- ¹¹ M. T. Hutchings, in: *Solid State Physics* Vol. 16, ed. F. Seitz and D. Turnbull, Academic Press, New York and London (1964) 227
- ¹² S. W. Lovesey, *Theory of Neutron Scattering from Condensed Matter*, Clarendon Press Oxford (1984)
- ¹³ M. Cwik, M. Benomar, T. Finger, Y. Sidis, D. Senff, M. Reuther, T. Lorenz and M. Braden, *Phys. Rev. Lett.* **102**, 057201 (2009)
- ¹⁴ K. Yamada, M. Matsuda, Y. Endoh, B. Keimer, R. J. Birgeneau, S. Onodera, J. Mizusaki, T. Matsuura and G. Shirane, *Phys. Rev. B* **39**, 2336 (1989)
- ¹⁵ P. G. Radaelli and S.-W. Cheong, *Phys. Rev. B* **66**, 094408 (2002)
- ¹⁶ M. Soda, M. Matsumoto, M. Månsson, S. Ohira-Kawamura, K. Nakajima, R. Shiina and T. Masuda, *Phys. Rev. Lett.* **112**, 127205 (2014)
- ¹⁷ Jens Jensen, *Phys. Rev. B* **79**, 014406 (2009)
- ¹⁸ Very recent experimental data on a high quality $x=0.25$ sample by A. Komarek, private communication, clearly shows a very narrow feature, which is in better agreement with the calculation result shown fig. 2